

# Three Dimensional Nanoscale Abrasive Cutting Simulation and Analysis for Single-Crystal Silicon Workpiece

Zone-Ching Lin<sup>1</sup> and Ren-Yuan Wang<sup>1</sup>

**Abstract:** The paper establishes a new three-dimensional quasi-steady molecular statics nanoscale abrasive cutting model to investigate the abrasive cutting behavior in the downpressing and abrasive cutting process of a workpiece in chemical mechanical polishing (CMP) process. The downpressing and abrasive cutting process is a continuous process. The abrasive cutting process is done after the single abrasive particle has downpressed and penetrated a workpiece to a certain depth of a workpiece. The paper analyzes the effects of the abrasive particles with different diameters on action force. It also analyzes the action force change of abrasive particles with different diameters on the projected area of unit contact face between abrasive particle and workpiece. The distribution of nanoscale equivalent stress and equivalent strain of the midsection of workpiece in abrasive cutting process are also analyzed. Furthermore, the special phenomena those are found in this paper, the one is the diameter of abrasive particle is greater, the action force on the projected area of its unit contact face is smaller and the other one is particular prominent regional action force in nanoscale abrasive cutting process. Besides, adopting the new molecular statics abrasive cutting model developed by the paper, the paper undergoes the simulation of same parameter conditions, and compares the simulation results with the related literature of using molecular dynamics method in order to prove that the new model developed by the paper is reasonable.

**Keywords:** Quasi-steady molecular statics, nanoscale abrasive cutting, equivalent stress, equivalent strain.

## 1 Introduction

Having been extensively applied to semiconductor process, chemical mechanical polishing (CMP) is one of the main techniques for acquisition of wafer flattening and nanoscale surface shape. Polishing is an abrasive cutting process being a

---

<sup>1</sup> NTUST, Taipei, Taiwan.

very complicated behavior. A thorough understanding of the basic behaviors of step-by-step abrasion and removal of material by abrasive particles is an important key to the machining of parts with excellent functions. To obtain excellent surface condition, abrasive particles have been gradually developed to be of nanoscale [Estragnat; Tang; Liang; Jahanmir; Pei; Martin (2004)], and even the depth of abrasion is also of nanoscale. Many of the problems and phenomena encountered in nanoscale abrasive cutting process cannot be explained merely by microscopic continuum model. If continuum mechanics is employed to study the characteristics under nanoscale, many problems would be encountered. Therefore, it is required to develop a physical model under atomic scale to further understand the physical mechanism under nanoscale.

As shown from the past studies [Belak and Stowers (1990); Kim and Moon (1995); Shen and Atluri (2004); Fang; Wu; Zhou; Hu (2007); Pei; Lu; Fang; Wu (2006)], molecular dynamics (MD) was applicable to the simulation analysis of nanoscale system. Among of them, Shen and Atluri (2004) proposed the analysis of atomic-level stress calculation and continuum-molecular system equivalence. Their paper mainly studied that “an equivalent continuum is defined for molecular dynamics (MD) particle systems, based on the definition of atomistic stress and in conjunction with the SPH technique.” Besides, the case analyzed in their paper only considered the elastic fields in the discussion of uniform applied deformation.

Nevertheless, due to the too small time step of MD being taken, a lot of calculation time had to be spent in simulation process, so the problem of calculation was created. But if the adopted time step of simulation was a too great value, there would be a problem that the sliding speed was also a too great value, which did not meet the actual physical phenomenon.

In view of this, some scholars gradually used molecular statics method to simulate nanoscale researches, attempting to solve the problems encountered by M.D. Kwon and Jung (2004) investigated the simulation of the material nature of atomic scale balance under static load, and proposed a model combining atoms with finite element method (FEM). This model was taken to simulate the problem of nanoscale defects. Telitchev and Vinogradov (2006) used quasi-static analysis method to investigate incomplete lattice structure. Their paper mentioned two different methods to find the static balance position. These two methods were minimum energy method, and selection of the time with relatively small force when atoms were moved. Each balanced state of lattice was expressed by a linear algebraic equation. Due to the displacement dependence of this equation, Inverse Broyden's Algorithm (IBA) was used to solve the system. If the bonding between two atoms was broken, it could be solved by Recursive Inverse Matrix Algorithm (RIMA). Based on the results acquired from minimum energy method, comparison was made to

prove the rationality of the theories. Jeng and Tan (2004) combined molecular statics method with minimum energy principles to form a structure to simulate the displacement and deformation process of nanoindentation. Minimum potential method was mainly used, and then the displacement control superposition method in FEM was also adopted to solve the relationship between the force and position of each atom. Theodosiou and Saravanos (2007), they focused on carbon nanotube to propose an analysis model of the bending deformation and stress of the nanotube of molecular mechanics based finite element after external force is borne. Their paper only considered the elastic moduli of the nanotube. Lin and Ye (2009) investigated the simulation of 2D nanocutting of different shape of diamond cutters cut the copper material, analysis the cutting action and cutting force et al. But this paper didn't consider the conditions of three dimension nanoscale abrasive cutting for single-crystal silicon workpiece.

In this paper, it simulates a new nanoscale abrasive cutting process during CMP abrasive process. It suppose that the abrasive particles firstly downpresses and penetrates the workpiece to a certain depth, and then moves the abrasive particle cutting workpiece. Because none of the related studies in the past literature has similar model. All of the relevant studies are either the nanoindentation studies with single abrasive particle penetrating the workpiece, or the studies with abrasive particles at a certain distance from outside the workpiece directly cutting of workpiece to a certain cutting depth.

Besides, the above mentioned references did not use molecular statics to simulate the above abrasive cutting process. Therefore, the paper develops a new nanoscale abrasive cutting model of molecular statics to simulate and investigate the abrasive cutting and machining behavior of diamond abrasive particles with three different sizes, as well as the distribution of their action force, stress and strain on silicon wafer. In order to prove that the new nanoscale abrasive cutting model of molecular statics developed by the paper is reasonable, the simulation results of the new theoretical model established by the paper are compared with those having the same parameters by References [Lin; Chen; Yang; Jian; Lai (2007) and Han; Hu; Yu (2009)]. Finally, it is proved that the new nanoscale abrasive cutting model of molecular statics developed by the paper is reasonable.

## **2 Three-dimensional quasi-steady nanoscale abrasive cutting model**

The new nanoscale abrasive cutting simulation model established by the paper is shown in Fig. 1. At a certain height from a workpiece, an abrasive particle downs to press on the workpiece in Y direction, and then penetrates the workpiece to a certain depth. After that, the abrasive particle moves and conducts abrasive cutting of the workpiece in X direction. In the past literature, there was no simulation model

being the same as the one established by the paper. The new model developed by the paper is closer to the actual CMP abrasive cutting model in practice.

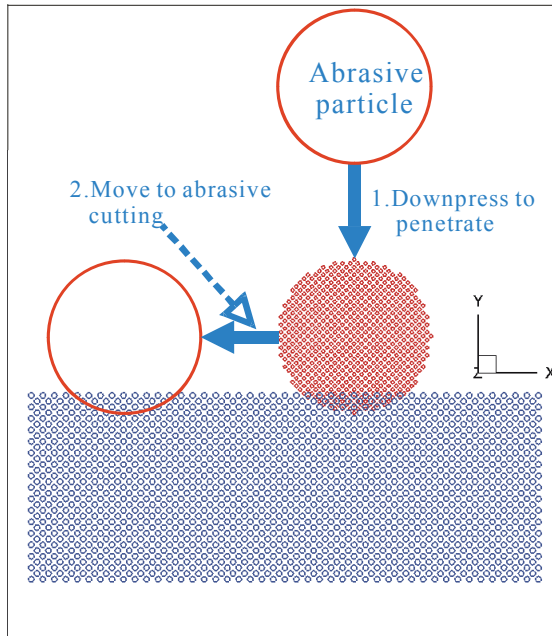


Figure 1: Schematic diagram of three-dimensional quasi-steady nanoscale abrasive cutting model.

The paper’s nanoscale abrasive cutting model of quasi-steady molecular statics adopts the Morse potential of two-bodied potential energy as the basis in the calculation of the action force of attractive force or repulsive force between atoms. When the distance between atoms is greater than a constant value, the action force between atoms calculate by Morse potential function decreases rapidly. Therefore, the constant value of  $r_c$  is so-called cut-off radius is defined. When the distance exceeds  $r_c$ , the action force is very small, so it can be ignored. Hence, the calculation items can be enormously simplified. When  $r_{ij}$ (distance between two atoms) is greater than 2.5 times of  $r_0$ (balance distance between two atoms), the potential energy is close to zero. Hence, the paper sets the cut-off radius  $r_c$  to be 2.5 times of  $r_0$ . The cut-off radius of Morse potential energy is expressed as equation (1)[Girifalco and Weizer (1959)]:

$$\begin{cases} \Phi(r_{ij}) = D \left\{ e^{-2\alpha(r_{ij}-r_0)} - 2e^{-\alpha(r_{ij}-r_0)} \right\}, & r \leq r_c \\ \Phi(r_{ij}) = 0, & r > r_c \end{cases} \quad (1)$$

$D$ : bonding energy

$\alpha$ : material parameter

$r_{ij}$ : distance between two atoms

$r_0$ : balance distance

After that, the negative value of function gradient of Morse potential energy is taken as the action force between two atoms. The action force of molecules is expressed as equation (2):

$$F(r_{ij}) = -\frac{\partial \Phi(r_{ij})}{\partial (r_{ij})} = 2D\alpha \left\{ e^{-2\alpha(r_{ij}-r_0)} - e^{-\alpha(r_{ij}-r_0)} \right\} \quad (2)$$

As inferred from equation (2), the action force can be get. After action force is obtained as equation (3), cut-off radius method is employed to increase a judgment whether the distance  $r_{ij}$  is greater than the parameter  $\delta$  of  $r_c$ . When the distance  $r_{ij}$  is greater than  $r_c$ , there is almost no potential energy function; by then, let  $\delta$  be 0. Contrarily, when the distance  $r_{ij}$  is smaller than  $r_c$ , action force will be produced; by then, let  $\delta$  be 1.

$$\vec{F}_i = \sum_{i=1}^n \vec{F}_{ij} \delta(r_{ij}) \quad (3)$$

if  $r_{ij} \geq r_c \rightarrow \delta=0$

else  $r_{ij} \leq r_c \rightarrow \delta=1$

The numerical value of the produced action force is divided into three axial component forces,  $\vec{F}_x$ ,  $\vec{F}_y$  and  $\vec{F}_z$ , with their relationship expressed in equation (4):

$$\vec{F}_i = \vec{F}_{x_i} + \vec{F}_{y_i} + \vec{F}_{z_i} \quad (4)$$

$\vec{F}_{x_i}$ : component force of action force in X direction

$\vec{F}_{y_i}$ : component force of action force in Y direction

$\vec{F}_{z_i}$ : component force of action force in Z direction

As indicated in Fig. 2, suppose that there is only a silicon workpiece atom Si-1 situated in the cut-off radius area of abrasive particle. With the Morse force of abrasive particle, slight displacement and deformation are caused to the silicon workpiece atom Si-1. Let the newly displaced position of the silicon workpiece atom be an unknown  $P(x,y,z)$ . Then, find the unknown displacement value created by this unknown  $P(x,y,z)$  to the abrasive particle atom and other silicon atoms inside the cut-off radius of atom Si-1. After that, substitute the unknown displacement distance in the Morse force equation of equation (3), find the Morse force vector created by  $P(x, y, z)$  to the abrasive particles and other silicon atoms inside the

cut-off radius of atom Si-1, and then decompose the unknown components in X, Y and Z directions. Find the sum of unknown forces in X direction created by the abovementioned  $P(x, y, z)$  to the abrasive particles and other silicon atoms inside the cut-off radius of atom Si-1. Also find the sum of forces in Y direction and the sum of forces in Z direction. Finally, let the sum of force components in X direction, the sum of force components in Y direction and the sum of force components in Z direction be zero, then a quasi-steady balance equation is established. The paper adopts Morse two-bodied potential energy function to explain the interaction force between si-si and si-c molecules of the 3D model, and the relative parameters of Morse force equation (2) for si-si and si-c are shown in Tab. 1 [Girifalco and Weizer (1959)].

Of course after abrasive cutting has been undergone for a period, there is more than one silicon workpiece atom affected by the Morse force of abrasive particles.

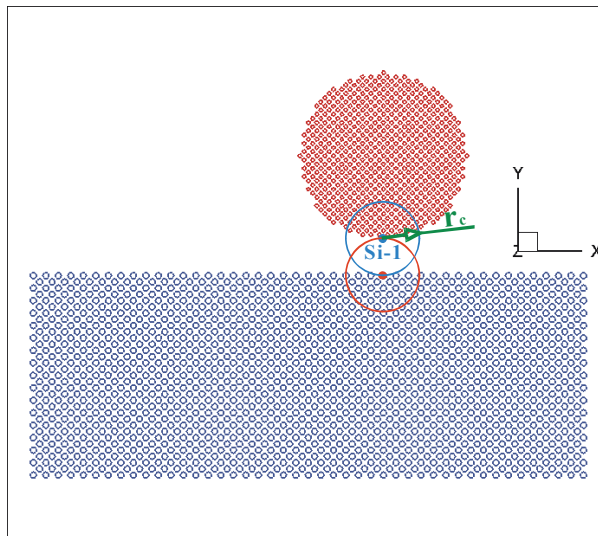


Figure 2: Schematic diagram of the area of cut-off radius  $r_c$ , implying to the affected area of silicon atoms

Table 1: Morse potential energy functions of silicon atom

	si-si	si-c
D: bonding energy (ev)	3.302	0.435
A: material parameter ( $\text{\AA}^{-1}$ )	0.7981	4.6487
$r_0$ : Balanced distance between atoms ( $\text{\AA}$ )	4.208	1.9475

The unknown force vector in the silicon workpiece affected by the Morse force of abrasive particles is added with the force vector created by the group of atoms to the silicon atoms inside the cut-off radius itself. Then, the sum of unknown force vectors can be acquired. The sum is decomposed to be component  $F_x$  in X direction, component  $F_y$  in Y direction and component  $F_z$  in Z direction respectively. Let each of the components be zero, then a quasi-steady balance equation is established, as shown in equation (5):

$$F_X = \sum_{i=1}^m \vec{F}_{ix}(r_{ij}) = \sum_{i=1}^m \sum_{j=1}^n F_x(r_{ij}) = 0 \quad (5)$$

$$F_Y = \sum_{i=1}^m \vec{F}_{iy}(r_{ij}) = \sum_{i=1}^m \sum_{j=1}^n F_y(r_{ij}) = 0$$

$$F_Z = \sum_{i=1}^m \vec{F}_{iz}(r_{ij}) = \sum_{i=1}^m \sum_{j=1}^n F_z(r_{ij}) = 0$$

i: number assigned to all the abrasive particle atoms being corresponding to the silicon atoms affected by Morse force of abrasive particles.

j: number assigned to the silicon atoms inside the cut-off radius after removal of the silicon atoms affected by Morse force of abrasive particles.

m: quantity of all the abrasive particle atoms being corresponding to the silicon atoms affected by Morse force of abrasive particles.

n: quantity of the silicon atoms inside the cut-off radius after removal of the silicon atoms affected by Morse force of abrasive particles.

$r_{ij}$ : distance from the  $j^{th}$  silicon atom in material to the  $i^{th}$  abrasive particle atom in cutting tool, and the distance from the  $j^{th}$  silicon atom to the  $i^{th}$  atom.

The differential expressions of components  $F_x$  in X direction,  $F_y$  in Y direction and  $F_z$  in Z direction used in this paper cannot be solved easily, making it difficult to construct equations. Hence, the paper proposes the concept of optimization to look for the optimal displaced position. To use optimization searching method to solve the optimal displaced position, the first thing to do is to determine a searching area. Since the feeding of each step in the paper does not exceed  $0.002\text{\AA}$ , and an atom cannot go through another atom easily to make it deformed, the paper supposes that each feeding does not exceed the distance of  $1/2$  lattice constant, and then searches the optimal force balance deformation and displaced position for each step of feeding. Hooke-Jeeves pattern search method[Hooke and Jeeves (1961)] is adopted. First of all, the starting point has to be defined. The silicon atom affected by Morse force of abrasive particles in each cutting step is taken as the starting point of the search. The increment of search is  $0.001\text{\AA}$ , and the convergence value

of force equilibrium  $\varepsilon = 10^{-6}$ . By following the above logic, the point of optimal displaced position for each step can be found. It is just the point of new force balance displaced position acceptable to us.

### 3 Calculation of equivalent stress and equivalent strain of nanoscale abrasive cutting model of three-dimensional quasi-steady molecular statics

When calculating the feeding of abrasive particles in each step, after the new position of each silicon atom is obtained, the paper selects the atom at the midsection of workpiece, which is just A-A cross-section shown in Fig. 3. The new position of each atom is compared with its original position, acquiring the displacement value of silicon atom. The relationship between displacement function and node in FEM is applies. Each silicon atom is regarded as a node. Furthermore, the equivalent strain of silicon atom element can be calculated. After that, the paper adopts the equation of relational curve acquired by regression from the equivalent strain and equivalent stress data simulated by Reference [Aly; Ng; Veldhuis; Elbestawi (2007)], and further calculates the numerical value of equivalent stress of silicon atom at this time.

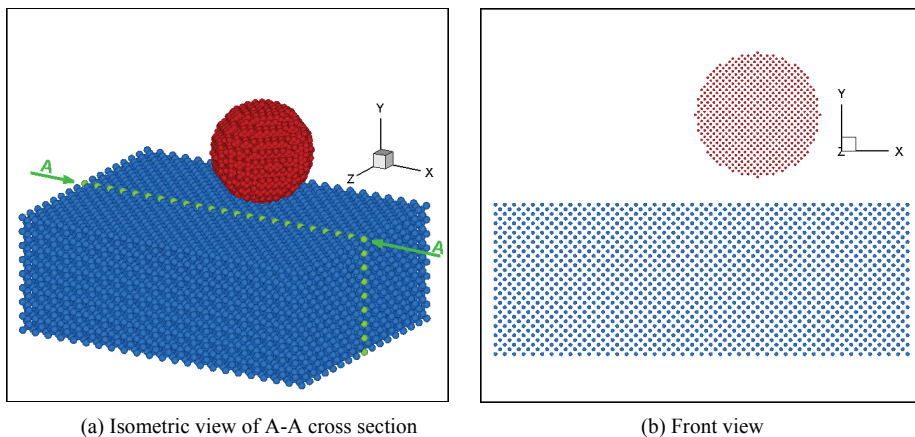


Figure 3: Structural diagram of abrasive particles and workpiece material: (a) Isometric view of A-A cross section ; and (b) Front view.

The paper adopts the constant strain triangle (CST) network of Lin and Huang (2004), the relationship between the displacement function of element and node in A-A cross-section of Fig. 3 is:

$$\{\phi\} = \begin{bmatrix} u(x,y) \\ v(x,y) \end{bmatrix} = \frac{1}{2A} \{N\} \{\delta\} \tag{6}$$

$[N]$ : shape function

$A$ : area of triangular element

Therefore, after inference, the relational equation between strain and displacement is as follows:

$$\{\varepsilon\} = \begin{bmatrix} \varepsilon_x \\ \varepsilon_y \\ \varepsilon_{xy} \end{bmatrix} = \{B\} \{\delta\} \quad (7)$$

where:  $\{\varepsilon\}$ : general strain matrix of element

$\{B\}$ : displacement-strain relational matrix

$\{\delta\}$ : node displacement matrix

Then, the displacement component of atoms can be acquired by using molecular statics. From the strain of element composed by the silicon atoms in equation, equivalent strain can be further calculated. As to the equation of relational curve between equivalent strain and equivalent stress, the paper adopts the regressed equation (10) of the relational curve between equivalent strain and equivalent stress of silicon single-crystal material simulated by Reference [Aly; Ng; Veldhuis; Elbestawi (2007)] as the foundation. Then, the relational curve between equivalent stress and equivalent strain to be required by this paper can be obtained. By using equation (8), together with the equivalent strain calculated above, the equivalent stress produced under the equivalent strain of each element can be calculated.

$$\bar{\sigma} = \begin{cases} 46.2108\bar{\varepsilon} + 13.8598, & \bar{\varepsilon} < 0.25 \\ -164.5613\bar{\varepsilon}^2 + 11.0263\bar{\varepsilon} + 9.7763, & 0 \leq \bar{\varepsilon} \leq 0.25 \\ 46.2108\bar{\varepsilon} + 13.8598, & \bar{\varepsilon} > 0.25 \end{cases} \quad (8)$$

$\bar{\sigma}$ : equivalent stress

$\bar{\varepsilon}$ : equivalent strain

In order to know the trend of change of equivalent strain and equivalent stress, the paper uses arithmetic mean to equalize the values of equivalent strain and equivalent stress of atoms to the node atoms, and calculates the equivalent strain and equivalent stress of atomic nodes. In this way, the trend of change of the contour of equivalent strain and equivalent stress can be drawn.

#### 4 Results and discussion

The new nanoscale abrasive cutting model of three-dimensional quasi-steady molecular statics developed by this paper simulates the abrasive cutting of single-crystal

silicon material by diamond abrasive particles. The considered diamond nanoscale abrasive particles are supposed to be spherical rigid bodies. In the related studies about chemical mechanical polishing (CMP) indicated in References [Estragnat; Tang; Liang; Jahanmir; Pei; Martin (2004); Han; Hu; Yu (2009) and Zhao; Chang (2002)], no matter of experimental studies [Estragnat; Tang; Liang; Jahanmir; Pei; Martin (2004)], or the induction and establishment of theoretical model, and the simulation of abrasive cutting of molecular dynamics [Han; Hu; Yu (2009)], the diameter of the used abrasive particles have reached nanoscale. In Reference [Han; Hu; Yu (2009)], the round edge radii of abrasive particles are 0nm, 1 nm, 1.5nm, 2 nm, 2.5 nm, 3nm and 3.5nm respectively. Therefore, the diameter of the abrasive particles used by the paper for simulation of abrasive cutting are also of nanoscale, with diameters being 21.72 Å, 28.96 Å and 36.2 Å respectively (just 6, 8 and 10 times of the lattice constant of carbon). These abrasive particles contain 915, 2,149 and 4,235 atoms respectively. The dimensions of single-crystal silicon workpiece material are 119.46 Å × 43.44 Å × 86.88 Å (its lengths in X, Y and Z directions are 22, 8 and 16 times of the silicon lattice constant), containing 23,887 atoms. The depth of abrasive cutting is 4.072Å. The parameters of simulation use by this paper as shown in Tab. 2. The setup of abrasive particles and the workpiece material to be abraded and cut are shown in Fig. 3.

#### 4.1 Verification of simulation

In order to prove that the new model constructed by the paper is reasonable, the paper refers to the simulation parameter conditions of References [Lin; Chen; Yang; Jian; Lai (2007) and Han; Hu; Yu (2009)], employs the theoretical model developed by the paper, and simulates the indentation and abrasive cutting of single-crystal silicon material by diamond abrasive particles. The action force in Y direction, which is just the thrust force, is compared with the nanoindentation load simulated by molecular dynamics used in References [Lin; Chen; Yang; Jian; Lai (2007) and Han; Hu; Yu (2009)]. When the indented and penetrated depth is 15Å, the numerical value of action force is about 2300nN. The paper adopts three-dimensional quasi-steady molecular statics to carry out simulation with parameters the same as those in Reference [Lin; Chen; Yang; Jian; Lai (2007)]. When the penetrated depth is the same as Reference [Lin; Chen; Yang; Jian; Lai (2007)], the action force in Y direction is 2199.95nN, having an error of 4.35% in between this result and Reference's [Lin; Chen; Yang; Jian; Lai (2007)].

Reference [Han; Hu; Yu (2009)] adopts molecular dynamics to simulate the material removal mechanism by CMP. For the adopted model, abrasive particles directly conduct abrasive cutting of workpiece to a certain depth, without simulation process of downpressing and penetrating the workpiece. The average cutting force of

Table 2: The parameters of simulation use by this paper

	Diamond abrasive particles		Single-crystal silicon workpiece		Abrasive cutting depth (Å)
	Diameter (Å)	Number of atoms	Dimension (Å <sup>3</sup> )	Number of atoms	
Case 1	21.72	915	119.46 × 43.44 × 86.88	23,887	4.072
Case 2	28.96	2,149			
Case 3	36.2	4,235			

Reference [Han; Hu; Yu (2009)] is about 150nN. The paper uses three-dimensional quasi-steady molecular statics to simulate the same parameters as Reference [Han; Hu; Yu (2009)], the simulation results of the average action force in X direction at stable convergence is 140.51nN, having an error of 6.33% between this result and Reference's [Han; Hu; Yu (2009)].

From the above verification, the error is within a reasonable and acceptable range. Therefore, the model constructed by the paper should be a reasonable and feasible model available for application to the simulation of abrasive cutting of single-crystal material by diamond abrasive particles. Subsequently, the study investigates the simulation result of downpressing prior to abrasive cutting.

#### ***4.2 Investigation of nanoscale abrasive cutting behavior***

The preliminary simulation of the study is that the coordinates of diamond abrasive particles in Y direction are set at the distance  $8\text{\AA}$  from above the silicon wafer, and the penetration depth of workpiece material is set to be  $4.072\text{\AA}$ . With the feeding of  $0.002\text{\AA}$  per step taken as the feeding condition of abrasive cutting, the paper carries out simulation of abrasive cutting of nanoscale single-crystal silicon material. The paper uses the front view and isometric view of the abrasive particles with diameter  $36.2\text{\AA}$  when they are at the  $6,036^{\text{th}}$  step of downpressing process of diamond abrasive particles and at the  $15,000^{\text{th}}$  step of cutting process of abrasive particles as shown in Fig. 4(a). When abrasive particle downpresses and penetrates the workpiece, ridges are produced at the workpiece with abrasive particles around. Especially by the left side of the abrasive particles, there is a protruding area at the top of the workpiece with ridges. As the abrasive particles are moving, abrading and cutting, the abrasive cutting phenomenon can be obviously seen. The cutting has side-flow phenomenon, and ridges are formed by the two sides of the machining path. Besides, as the abrasive particles keep on conducting abrasive cutting, the accumulation of chips is more obvious at the front end of the abrasive particles. Similar phenomenon also occurs to the abrasive particles with other two different diameters.

#### ***4.3 Investigation of nanoscale abrasive cutting action force***

Figures 5, 6 and 7 show the action forces produced by diamond abrasive particles on single-crystal silicon in X, Y and Z direction within the total feeding length  $30\text{\AA}$  of abrasive cutting. Every 2,500 abrasive cutting steps is taken as an indication point, implying to a cutting feeding of  $5\text{\AA}$  taken as an indication point. This way is convenient for observing the action force change of single-crystal silicon material. The so-called action force in X direction refers to the so-called cutting force in general cutting process; the action force in Y direction refers to thrust force, and

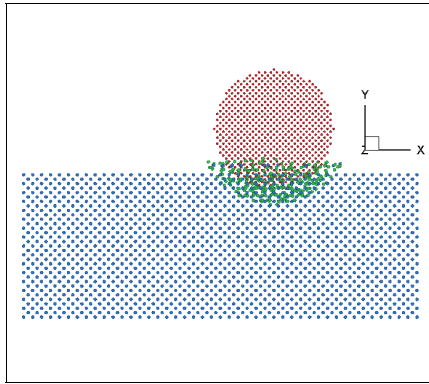
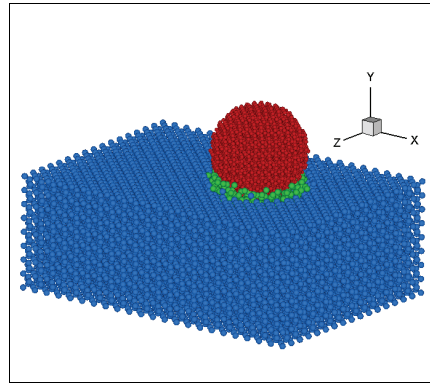
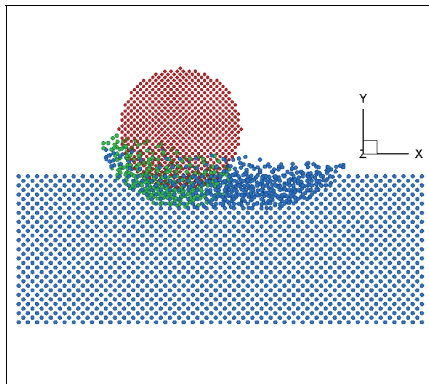
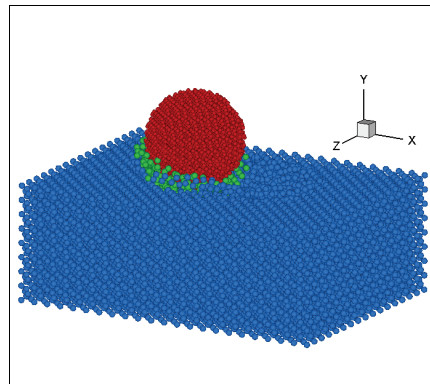
(a) Front view of the 6,036<sup>th</sup> step (feeding length 12.072Å)(b) Isometric view of the 6,036<sup>th</sup> step (feeding length 12.072Å)(c) Front view of the 15,000<sup>th</sup> step (feeding length 30Å)(d) Isometric view of the 15,000<sup>th</sup> step (feeding length 30Å)

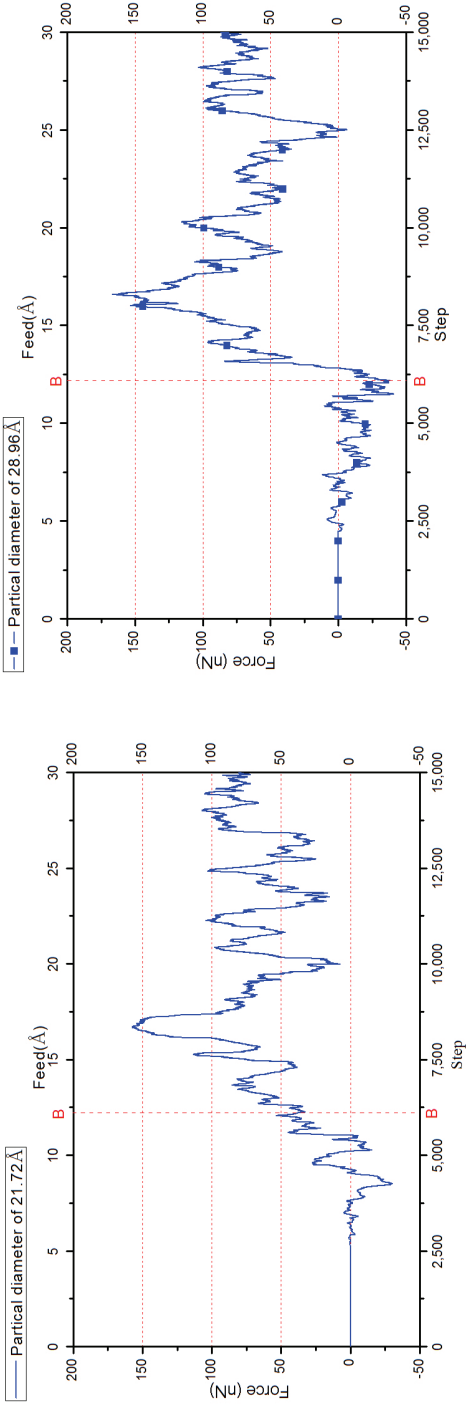
Figure 4: The 6,036<sup>th</sup> step (feeding length 12.072Å) in downpressing process, the 15,000<sup>th</sup> step (feeding length 30Å) in abrasive cutting process by the abrasive particles with diameter 36.2Å: (a) Front view of the 6,036<sup>th</sup> step; (b) Isometric view of the 6,036<sup>th</sup> step; (c) Front view of the 15,000<sup>th</sup> step; and (d) Isometric view of the 15,000<sup>th</sup> step

the action force in Z direction refers to normal force. In the figures, the step before B-B line refers the downpressing and penetration process of workpiece by abrasive particles in Y direction; and the step after B-B line refers to the abrasive cutting process of workpiece by abrasive particles in X direction after the abrasive particles have downpressed to the penetration depth 4.072Å of workpiece as set by the paper. The paper defines that the attraction force between diamond abrasive particles and single-crystal silicon workpiece material is a negative value, and the repulsive force between diamond abrasive particles and single-crystal silicon workpiece material

is a positive value. The cutting forces in the abrasive cutting process is analyzed and investigated as follows:

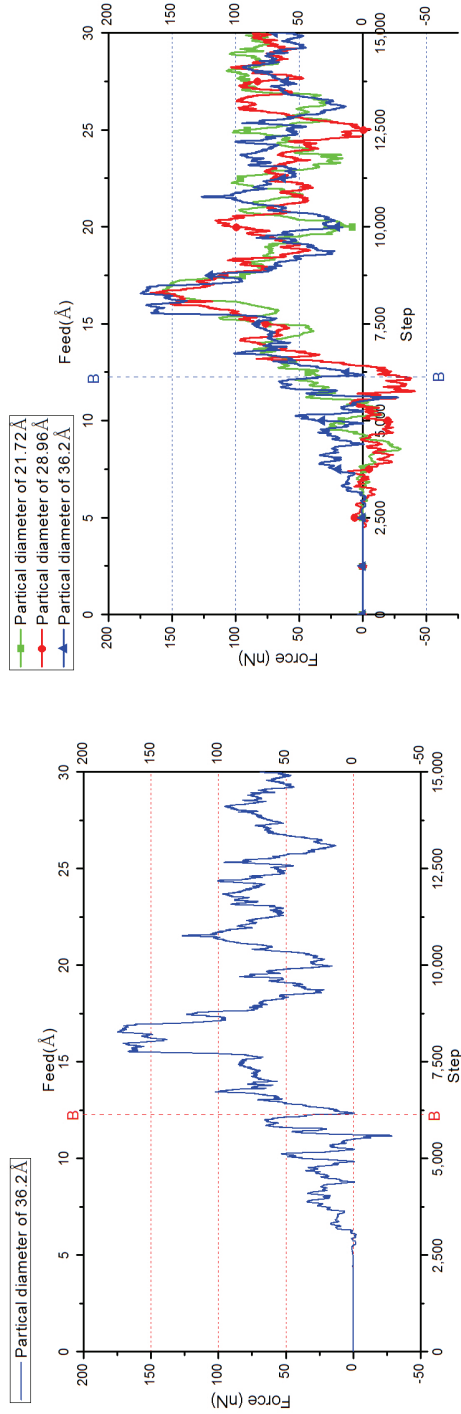
As shown in Fig. 5(c), the area from the 7,900<sup>th</sup> step (feeding length 15.8Å) to the 8,700<sup>th</sup> step (feeding length 17.4Å) of the abrasive particles with diameter 36.2Å is a zone with greater values of action forces occurred in X direction. This is mainly related to the new nanoscale abrasive cutting model constructed by the paper. The greatest difference of the new nanoscale abrasive cutting model of the paper from that of the literature is that the abrasive particles firstly downpresses and penetrates the workpiece prior to the abrasive cutting of the workpiece. The action forces in such X direction are of greater values. Fig. 9 is a front view of the abrasive particles with diameter 36.2 Å when they downpress the abrasive depth set by the paper. As observed from the left side of the abrasive particles in the figure, since ridges are produced at the workpiece by abrasive particles in the downpressing process, the top end of this part has a protruding zone. The width of this zone is 1.64Å, and the width between the right end of the protruding zone with ridges and the abrasive particles is 3.76Å. These two numerical values are divided by the feeding of 0.002Å per step, and then added with the number of steps in downpressing process, being 7,916 and 8,736 steps respectively. The results are checked with the curve in Fig. 5, and they just lay in the zone with greater values of action force appeared in X direction. As known from here, after abrasive particles has downpressed and penetrated the workpiece, and then start to cut in X direction move to the protruding zone of the workpiece with ridges at its top end, it is just the zone with relatively greater values of action force produced in X direction. This is a special phenomenon that is found in the paper, no such phenomenon has been analyzed in the past literature. But in the simulation process of this paper, it is found that in the abrasive cutting process with abrasive particle downpressing the workpiece prior to moving of it, such kind of phenomenon also occur to both the abrasive particles with diameters 21.72 Å and 28.96 Å.

Comparison of the action forces of the abrasive particles with three different diameters in different directions: The action forces of the abrasive particles with three different diameters in Y direction at the 6,036<sup>th</sup> step (feeding length 12.072Å) of downpressing process and the average action force in X and Y directions as the abrasive cutting situation appears to be stable, referring to the time after the 9,000<sup>th</sup> step (feeding length 18Å) of abrasive cutting, are rearranged well in Fig. 10. As seen from Fig. 10, in the downpressing process, the action force in Y direction increases with the enlargement of abrasive particles in diameter. In the abrasive cutting process, the action forces of the abrasive particles with three different diameters in Y direction increases with the enlargement of abrasive particles in diameter, and so are the action forces in X direction. However, the action force difference in

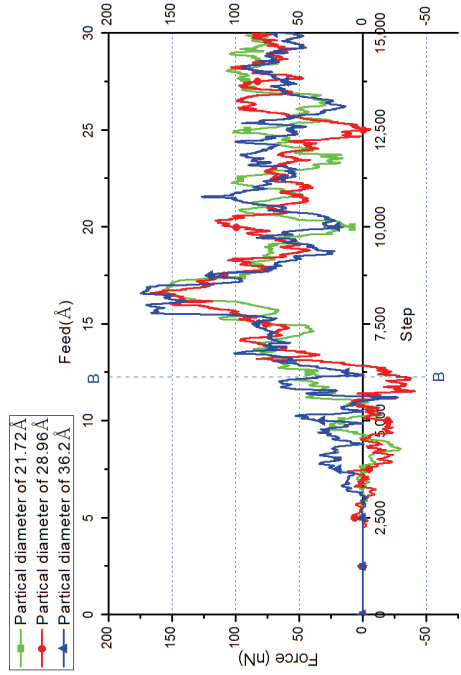


(a) Particle diameter of 21.72 Å in X direction

(b) Particle diameter of 28.96 Å in X direction



(c) Particle diameter of 36.2 Å in X direction



(d) Comparison of three different particle diameters in X direction

Figure 5: Action force in X direction: (a) particle diameter of 21.72 Å; (b) particle diameter of 28.96 Å (c) particle diameter of 36.2 Å; (d) Comparison of three different particle diameters

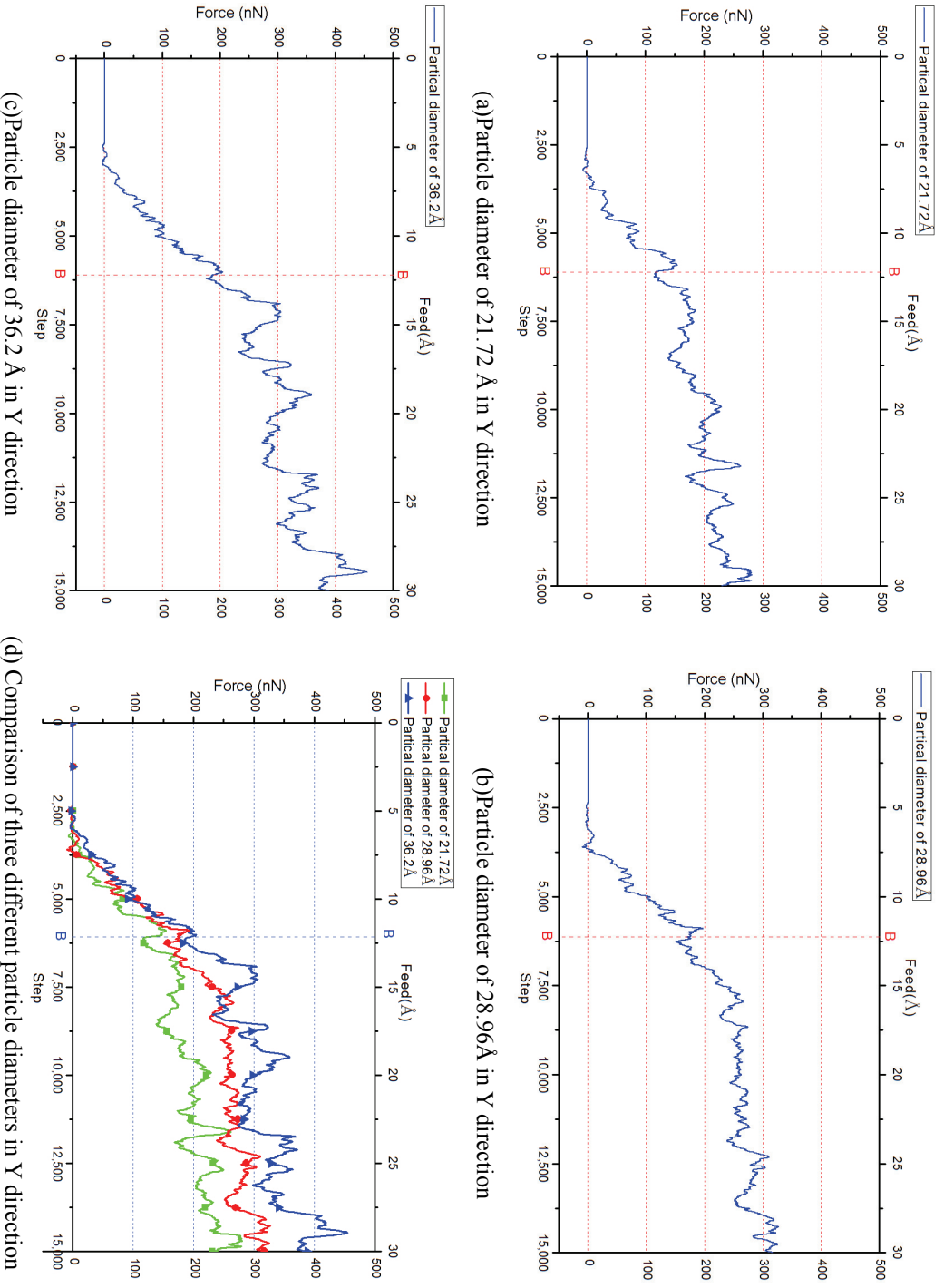
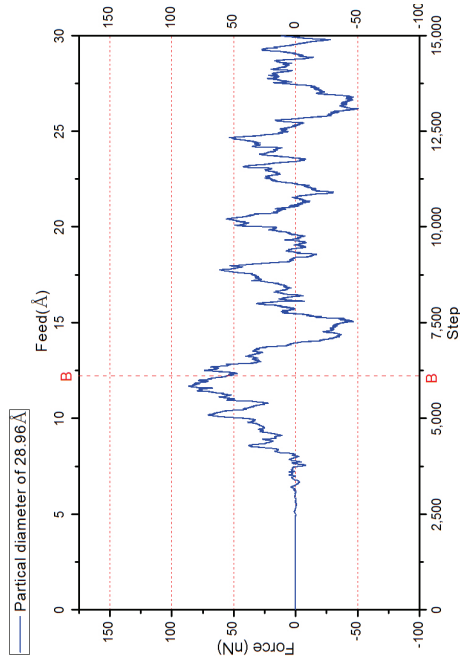
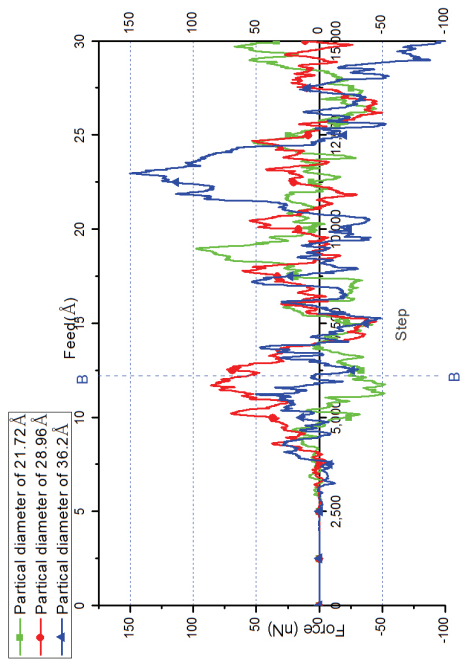


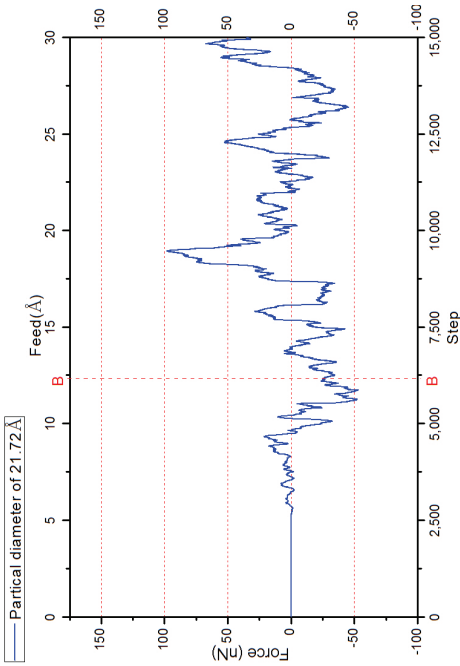
Figure 6: Action force in Y direction: (a) particle diameter of 21.72 Å; (b) particle diameter of 28.96 Å (c) particle diameter of 36.2 Å; (d) Comparison of three different particle diameters



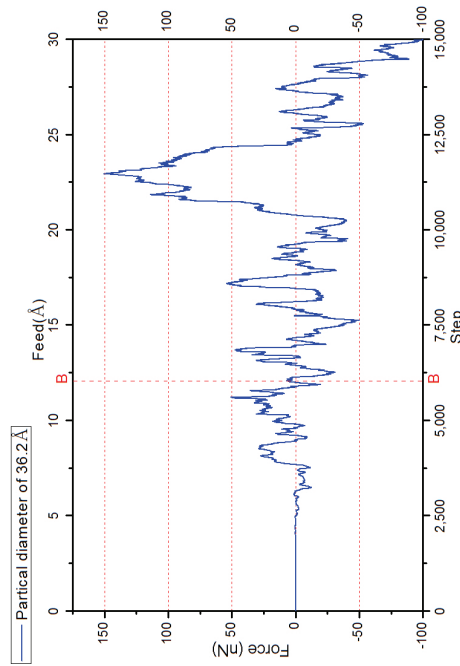
(a) Particle diameter of 21.72 Å in Z direction



(b) Particle diameter of 28.96 Å in Z direction



(c) Particle diameter of 36.2 Å in Z direction



(d) Comparison of three different particle diameters in Z direction

Figure 7: Action force in Z direction: (a) particle diameter of 21.72 Å; (b) particle diameter of 28.96 Å (c) particle diameter of 36.2 Å; (d) Comparison of three different particle diameters

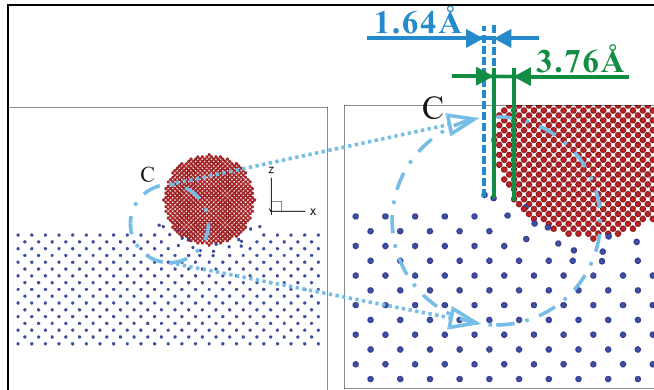


Figure 9: Shape of ridges on workpiece at the front end of the abrasive particles when the abrasive particles with diameter 36.2 Å are at the 6.036<sup>th</sup> step(feeding length 12.072Å) in the downpressing process.

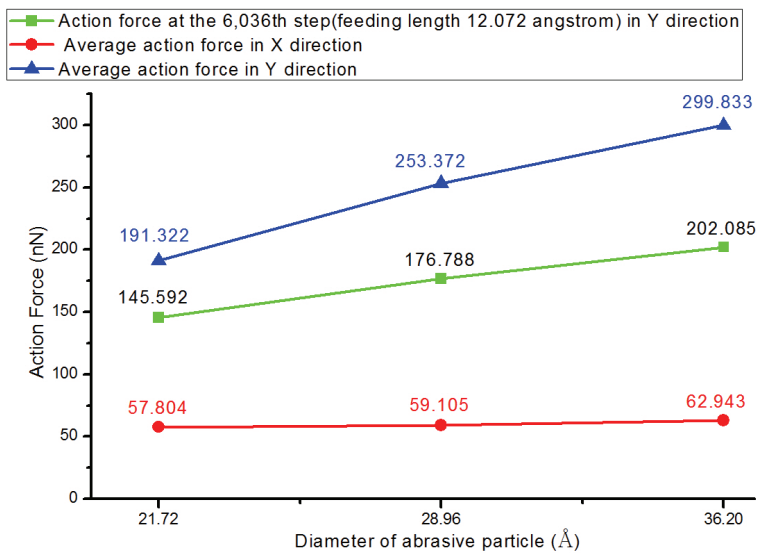


Figure 10: Average action force of the abrasive particles with three different diameters in X and Y directions in the abrasive cutting process

Y direction is greater, and the action force difference in X direction is smaller. Its reason is related to the size of projected area of the contact face between the spherical abrasive particle and the workpiece to different directions, as shown in Fig. 11. Figure 12 shows the projected area of the contact face between the workpiece and the abrasive particles with three different diameters in X and Y directions when the abrasive particles have downpressed the workpiece to a penetration depth  $4.072\text{\AA}$ . As known from Fig. 12, the greater of the projected area of contact face, the greater of the action force. Although the action force in Z direction has been fluctuating up and down on the coordinate axis, the average value is close to zero. This is because the abrasive cutting path of this paper is a straight line. Thus, the contact areas at the two sides of the abrasive particles in Z direction are similar in size. But the magnitude of change of the abrasive particles with greater diameter is also greater.

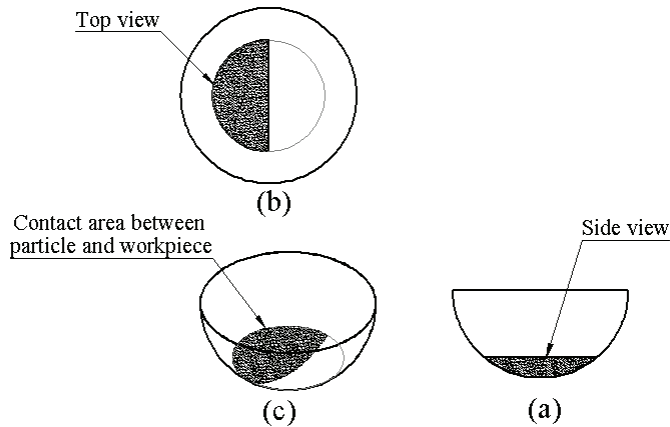


Figure 11: Project area of contact face: (a) Projected area of contact face by the right side; (b) Projected area of contact face in the direction of top view; and (c) Contact area between abrasive particles and workpiece.

We further divide the average action forces in X and Y directions by the projected area of contact face in X and Y directions. As found in the numerical values in Fig. 12, there are three kinds of abrasive particles with different diameters. No matter in X direction or Y direction, the action force of the abrasive particles with larger diameters on the projected area of their unit contact face is smaller than that of the abrasive particles with smaller diameters. As a result, as the diameter of abrasive particles is greater, the action force on the projected area of their unit contact face is smaller. This is a special phenomenon that is found in this paper.

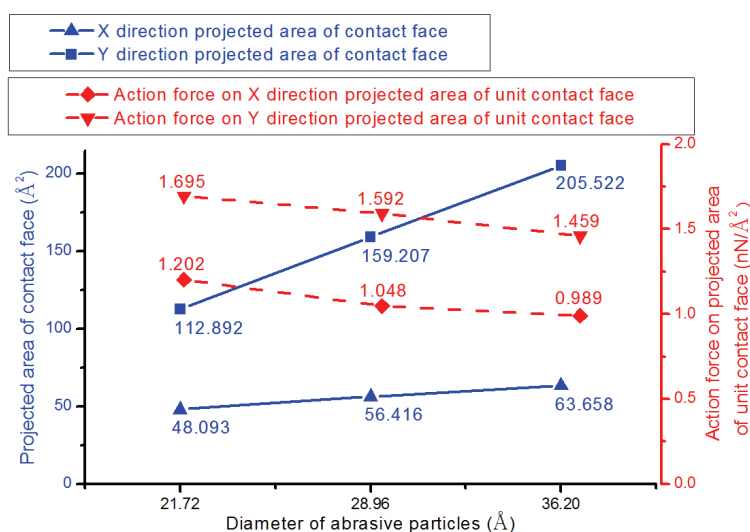


Figure 12: Projected area of contact face of the abrasive particles and action force on projected area of unit contact face of the abrasive particles in X and Y directions with three different diameters.

#### 4.4 Analysis of equivalent stress and equivalent strain

Figures 13, 14, and 15 show the observed distribution trend of equivalent strain and equivalent stress in the midsection of the workpiece (please see the A-A cross-section in Fig. 3) that three different abrasive particles diameter are at the 6,036<sup>th</sup> step (feeding length 12.072 Å) of the downpressing process and at the 15,000<sup>th</sup> step (feeding length 30 Å) of abrasive cutting process. The form of distribution is very close to the spherical shape of abrasive particles. As the penetration depth of workpiece is greater, the values of equivalent strain and equivalent stress are smaller. At the 15,000<sup>th</sup> (feeding length 30 Å) step of the abrasive cutting, the height of accumulated chips by the left side of the cross-section curve is higher. This is just like the abrasive cutting of the workpiece in X direction, or in the same direction towards the left side in the figure, when the abrasive particle downpresses and penetrates to a certain depth. As the abrasive cutting continues, more workpiece atoms are accumulated by the left side. Besides, at the place close to the root of the chips on the left side, the distribution trends of its equivalent strain and equivalent stress both appear in island shape. With the diameter increase of abrasive particles, the island-shaped distribution of equivalent stress and equivalent strain gradually moves upwards towards the top end of chips

Besides, in times of the abrasive cutting by the diamond abrasive particles with diameter 36.2Å, the greatest numerical value of equivalent strain produced is around 0.9, and the greatest numerical value of equivalent stress is around 55.45GPa. In times of the abrasive cutting by the diamond abrasive particles with diameter 29.86Å, the greatest numerical value of equivalent strain produced is around 0.85, and the greatest numerical value of equivalent stress is around 53.14GPa. In times of the abrasive cutting by the diamond abrasive particles with diameter 21.72Å, the greatest numerical value of equivalent strain produced is around 0.8, and the greatest numerical value of equivalent stress is around 50.83GPa. As the diameter of abrasive particles increase, the greatest values of both equivalent stress and equivalent strain on A-A cross-section are also slightly increased. At the same time, the distribution area of equivalent stress and equivalent strain is also enlarged with the increase of the diameter of abrasive particles.

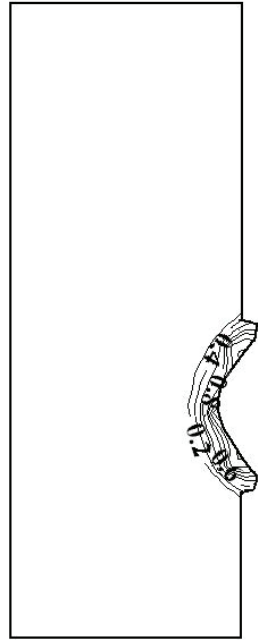
## **5 Conclusion**

The paper uses a new three-dimensional quasi-steady molecular statics to simulate the abrasion of single-crystal silicon material by nanoscale diamond abrasive particles, and observes the effects of the abrasive particles with three different diameters on the abrasive cutting behavior. According to the simulation results, the following conclusions are drawn:

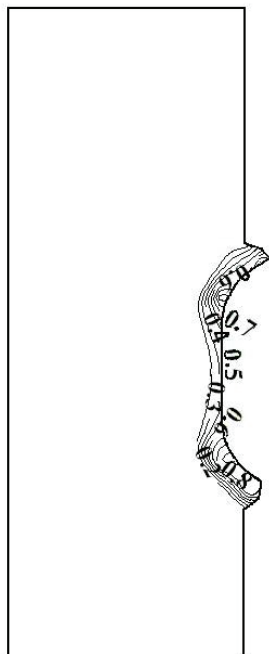
In the abrasive cutting process, side-flow phenomenon of chips can be obviously seen, and ridges are produced by the two sides of the machining path. As the abrasive cutting continues, the phenomenon of chip accumulation at the front end of abrasive particles is more obvious. Similar phenomenon also occurs to the abrasive particles with three different diameters.

In the downpressing and penetration process of workpiece by abrasive particles, ridges are produced at the workpiece with abrasive particles by the left side. When the abrasive particles move leftwards and the abrasive cutting reaches the ridge position of the workpiece, there appears an area with greater action force in X direction. Similar phenomenon also occurs to the abrasive particles with three different diameters. This is a special phenomenon that is found in this paper.

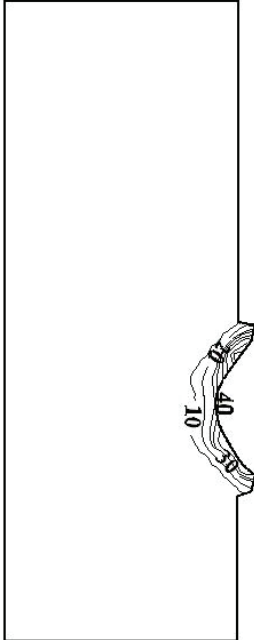
Regarding the action forces produced by the abrasive particles with three different diameters on single-crystal silicon material, the action forces in X and Y directions are greater; the action force of the abrasive particles with greater diameter is greater; the action force of the abrasive particles with smaller diameter is smaller; and the diameter of abrasive particle is greater, the action force on the projected area of its unit contact face is smaller. This is another special phenomenon that is found in this paper.



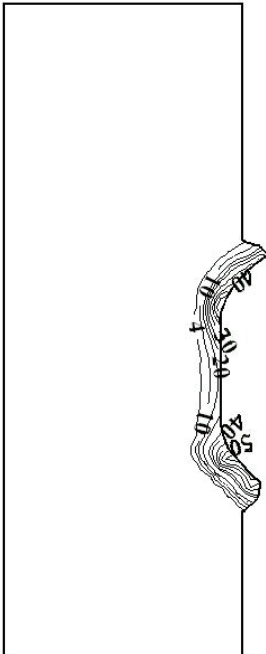
(a) Equivalent strain  $\bar{\epsilon}$  at the 6,036<sup>th</sup> step(feeding length 12.072Å)



(b) Equivalent strain  $\bar{\epsilon}$  at the 15,000<sup>th</sup> step(feeding length 30Å)



(c) Equivalent stress  $\bar{\sigma}$  at the 6,036<sup>th</sup> step(feeding length 12.072Å)



(d) Equivalent stress  $\bar{\sigma}$  at the 15,000<sup>th</sup> step(feeding length 30Å)

Figure 13: A-Å cross-section of abrasive particles with diameter 21.72 Å: (a) Equivalent strain  $\bar{\epsilon}$  at the 6,036<sup>th</sup> step(feeding length 12.072Å); (b) Equivalent strain  $\bar{\epsilon}$  at the 15,000<sup>th</sup> step(feeding length 30Å); (c) Equivalent stress  $\bar{\sigma}$  at the 6,036<sup>th</sup> step(feeding length 12.072Å); and (d) Equivalent stress  $\bar{\sigma}$  at the 15,000<sup>th</sup> step(feeding length 30Å)

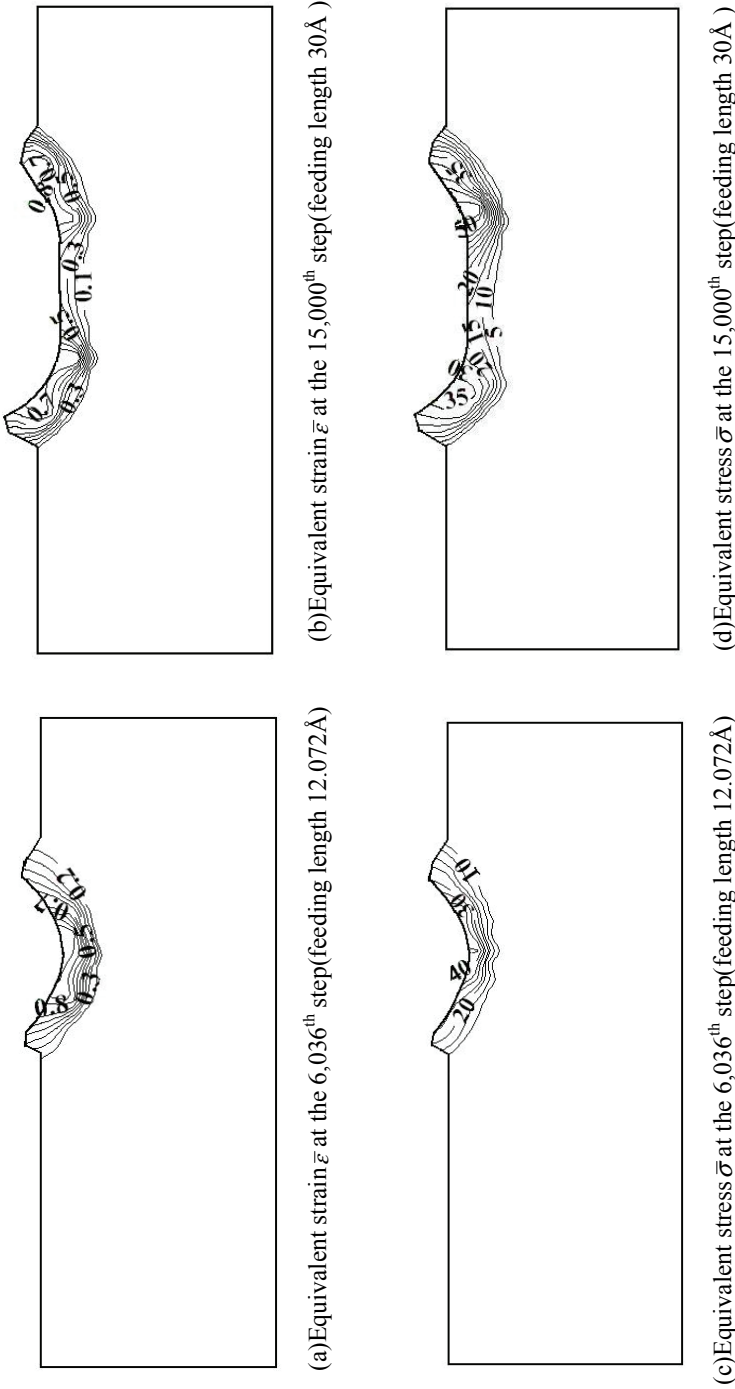


Figure 14: A-A cross-section of abrasive particles with diameter 28.96 Å: (a) Equivalent strain  $\bar{\epsilon}$  at the 6,036<sup>th</sup> step (feeding length 12.072 Å); (b) Equivalent strain  $\bar{\epsilon}$  at the 15,000<sup>th</sup> step (feeding length 30 Å); (c) Equivalent stress  $\bar{\sigma}$  at the 6,036<sup>th</sup> step (feeding length 12.072 Å); and (d) Equivalent stress  $\bar{\sigma}$  at the 15,000<sup>th</sup> step (feeding length 30 Å)

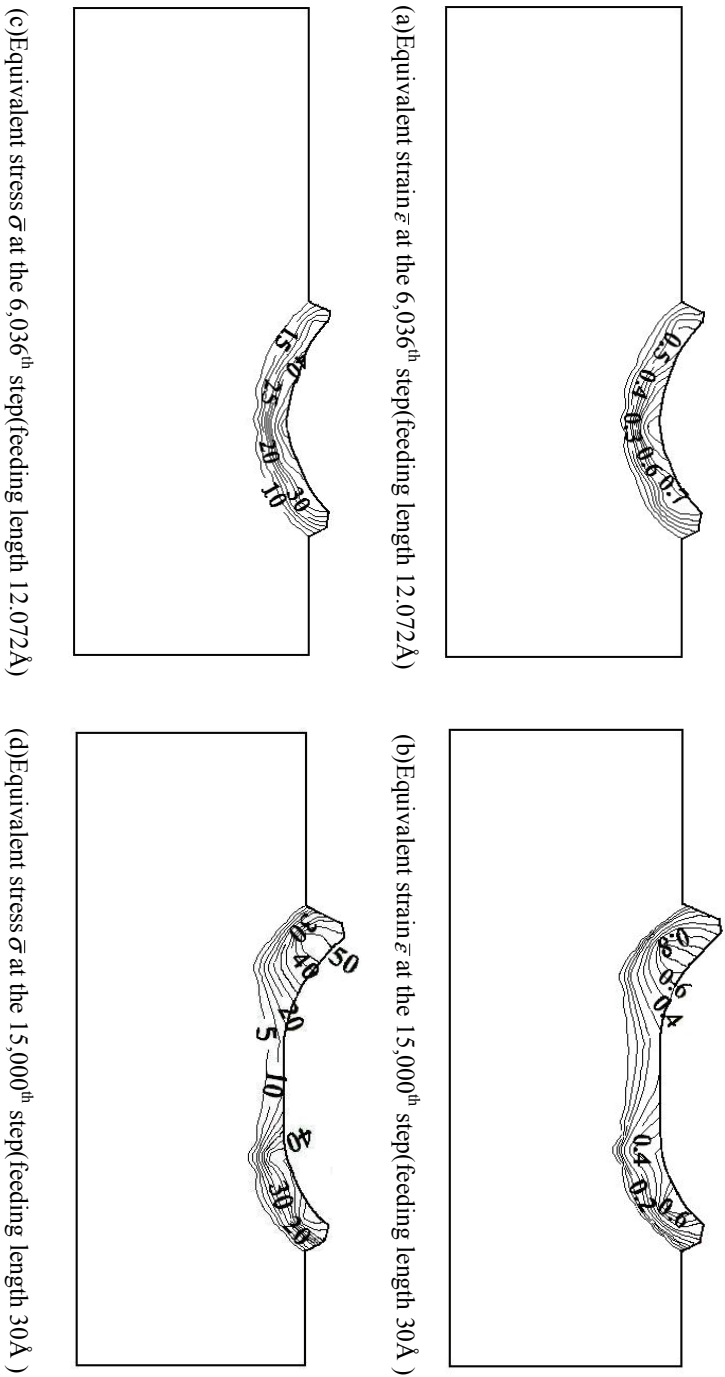


Figure 15: A-Å cross-section of abrasive particles with diameter 36.2 Å: (a)Equivalent strain  $\bar{\epsilon}$  at the 6,036<sup>th</sup> step(feeding length 12.072Å); (b)Equivalent strain  $\bar{\epsilon}$  at the 15,000<sup>th</sup> step(feeding length 30Å); (c)Equivalent stress  $\bar{\sigma}$  at the 6,036<sup>th</sup> step(feeding length 12.072Å); and (d)Equivalent stress  $\bar{\sigma}$  at the 15,000<sup>th</sup> step(feeding length 30Å)

The numerical value of equivalent stress and the affected area produced by the abrasive particles with greater diameters are slightly greater than those produced by the abrasive particles with smaller diameters.

**Acknowledgement:** The authors thank National Science Council (grant number NSC-96-2221-E-011-106-MY3 and NSC-98-2221-E-011-033-MY3) supporting this research.

## References

- Estragnat, E.; Tang, G.; Liang, H.; Jahanmir, S.; Pei, P.; Martin, J. M.** (2004): Experimental Investigation on Mechanisms of Silicon Chemical Mechanical Polishing. *Journal of Electronic Materials*, Vol. 33, No. 4, pp. 334-339.
- Belak, J.; Stowers, I. F.** (1990): A Molecular Dynamics Model of the Orthogonal Cutting Process. *Proc. Am. Soc., Precision Eng.*, Vol. 389, pp. 76-79.
- Kim, J. D.; Moon, C. H.** (1995): A study on microcutting for the configuration of tools using molecular dynamics, *Journal of Materials Processing Technology*, Vol. 59, No. 4, pp. 309-314.
- Fang, F. Z. ; Wu, H.; Zhou, W.; Hu, X. T.** (2007): A study on mechanism of nano-cutting single crystal silicon. *Journal of Materials Processing Technology*, Vol. 184, No. 1-3, pp. 407-410.
- Pei, Q. X.; Lu, C.; Fang, F. Z.; Wu, H.** (2006): Nanometric cutting of copper: A molecular dynamics study. *Computational Materials Science*, Vol. 37 (2006), No. 4, pp. 434-441.
- Kwon, Y. W.; Jung, S. H.** (2004): Atomic model and coupling with continuum model for static equilibrium problems. *Computers and Structures*, Vol. 82, September/October, Computational Structures Technology, pp. 1993-2000.
- Telitchev, I. Y.; Vinogradov, O.** (2006): A method for quasi-static analysis of topologically variable lattice structures. *International Journal of Computational Methods*, Vol. 3, March, pp. 71-81.
- Jeng, Y. R.; Tan, C. M.** (2004): Study of Nanoindentation Using FEM Atomic Model. *Journal of Tribology*, Vol. 126, pp. 767-774.
- Theodosiou, T. C.; Saravanos, D. A.** (2007): Molecular mechanics based finite element for carbon nanotube modeling. *CMES: Computer Modeling in Engineering & Sciences*, Vol. 19, No. 2, 121-134.
- Lin, Z. C.; Ye, J. R** (2009): Quasi-steady molecular statics model for simulation of nanoscale cutting with different diamond cutters. *CMES: Computer Modeling in Engineering & Sciences*, Vol.50, No.3, pp.227-252.

**Inamura, T.; Takezawa, N.** (1991): Cutting Experiments in a Computer Using Atomic Models of a Copper Crystal and a Diamond Tool. *Int. J. Japan Soc. Prec. Eng.*, Vol. 25, No. 4, pp. 259-266.

**Inamura, T.; Takezawa, N.** (1992): Atomic-Scale Cutting in a Computer Using Crystal Models of Copper and Diamond. *Annals of the CIRP*, Vol. 41, No. 1, pp. 121-124.

**Lin, Z. C.; Huang, J. C.** (2004): A nano-orthogonal Cutting Model Based on a Modified Molecular Dynamics Technique. *Nanotechnology*, Vol. 15, pp. 510-519.

**Shen, S.; Atluri, S. N.** (2004): Atomic-level Stress Calculation and Continuum-Molecular System Equivalence. *CMES: Computer Modeling in Engineering & Sciences*, Vol. 6, No. 1, pp. 91-104.

**Lin, Y. -H.; Chen, T. C.; Yang, P. F.; Jian, S. R.; Lai, Y. S.** (2007): Atomic-level simulations of nanoindentation-induced phase transformation in mono-crystalline silicon. *Applied Surface Science*, Vol. 254, pp. 1415–1422.

**Han, X.; Hu, Y.; Yu, S.** (2009): Investigation of material removal mechanism of silicon wafer in the chemical mechanical polishing process using molecular dynamics simulation method, *Appl. Phys. A*, Vol. 95, pp. 899–905.

**Girifalco, L. A.; Weizer, V. G.** (1959): Application of the Morse Potential Function to Cubic Metals. *Phys. Rev.*, Vol. 114, pp. 687-690.

**Hooke, R.; Jeeves, T. A.** (1961): Direct search solution of numerical and statistical problems. *Journal of the Association for Computing Machinery*, Vol. 8, pp. 212-229.

**Aly, M. F.; Ng, E.; Veldhuis, S. C. ;Elbestawi, M. A.** (2007): Prediction of cutting forces in the micro-machining of silicon using a hybrid molecular dynamic-finite element analysis force model. *International Journal of Machine Tool & Manufacture*, pp.1729-1737.

**Zhao, Y.; Chang, L.** (2002): A micro-contact and wear model for chemical–mechanical polishing of silicon wafers. *Wear*, Vol. 252, pp. 220–226.